atmosphere

MDPI

*Article*

# Characteristics of Observed Electromagnetic Wave Ducts in Tropical, Subtropical, and Middle Latitude Locations

**Sandra E. Yuter *,†, McKenzie M. Sevier †, Kevin D. Burris †,‡ and Matthew A. Miller †**

Department of Marine, Earth and Atmospheric Sciences, North Carolina State University, Raleigh, NC 27695, USA; kevin.burris@afacademy.af.edu (K.D.B.); mamille4@ncsu.edu (M.A.M.)

* Correspondence: seyuter@ncsu.edu

† These authors contributed equally to this work.

‡ Current address: Department of Physics and Meteorology, US Air Force Academy, Colorado Springs, CO 80840, USA.

**Abstract:** Where and at what altitudes electromagnetic wave ducts within the atmosphere are likely to occur is important for a variety of communication and military applications. We examined the modified refractivity profiles and wave duct characteristics derived from nearly 50,000 observed upper air soundings obtained over four years from seven tropical and subtropical islands, as well as middle latitude sites at four US coastal locations, three sites near the Great Lakes, and four US inland sites. Across all location types, elevated ducts were found to be more common than surface-based ducts, and the median duct thicknesses were ∼100 m. There was a weak correlation between duct thickness and strength and, essentially, no correlation between the duct strength and duct base height. EM ducts more frequently occurred at the tropical and subtropical island locations (∼60%) and middle latitude coastal locations (70%) as compared to the less than 30% of the time that occurred at the Great Lake and US inland sites. The tropical and subtropical island sites were more likely than the other location types to have ducts at altitudes higher than 2 km, which is above the boundary layer height.

**Keywords:** modified refractivity; wave duct; trapping layer; upper air sounding



Academic Editor: Stephan Havemann

Received: 29 January 2025
Revised: 10 March 2025
Accepted: 12 March 2025
Published: 17 March 2025

**Citation:** Yuter, S.E.; Sevier, M.M.; Burris, K.D.; Miller, M.A. Characteristics of Observed Electromagnetic Wave Ducts in Tropical, Subtropical, and Middle Latitude Locations. *Atmosphere* **2025**, *16*, 336. https://doi.org/10.3390/atmos16030336



## 1. Introduction

Atmospheric refraction bends electromagnetic (EM) waves when those waves traverse gradients in temperature and humidity [1–4]. In general, the refractive index of Earth's atmosphere decreases with increasing height and, as a consequence, beam paths bend downward relative to the surface compared to their path in a vacuum. Profiles of refractive index permit calculations of EM beam paths. Adjacent atmospheric layers with distinct temperature and humidity characteristics are bounded by sharp gradients in a refractive index. In these circumstances, the beam paths can be ducted, wherein the waves are guided within a horizontal layer, which allows them to travel further than they would in normal conditions. Temperature inversions, where temperature increases with increasing altitude, can yield trapping layers within ducts if the gradients in temperature and humidity are strong enough. Ducting can be caused by subsidence aloft, boundary layer inversions, or cooling near the surface, such as by nocturnal radiation inversions over land or warm dry air moving over a cooler body of water [5]. In calm, stable conditions over ocean, the air, when in contact with the sea surface, can become saturated, yielding ducting conditions of ∼10 m in thickness [4]. Evaporative downdrafts from precipitating clouds can also yield trapping layers at any altitude below cloud base. Surface cold pools originating from

evaporative downdrafts will spread laterally, so trapping layers associated with them will vary in height with time.

Previous work has extensively addressed the theory of EM refraction [1,2,4,6]. The range of frequencies that can become trapped is a function of duct thickness. Extended range propagation is more common at higher microwave frequencies as compared to lower microwave frequencies. Inversion methods estimate refractivity profiles from the measured signal and wave propagation models (see, e.g., [7]). Stable layers conducive to ducting can form in the marine atmosphere surface layer when warm offshore flow, or flow originating over warm currents (such as the Gulf Stream), traverses over cooler SSTs [8,9]. Elevated ducts are more commonly associated with the warm sectors of extratropical cyclones than other sectors, regardless of the storm's association with an atmospheric river [10].

Based on global forecast models, the highest ducting probabilities are found in the Arabian Sea, NW Africa, and in persistent marine stratocumulus conditions in the subtropics; this includes regions off the coasts of California and Mexico, Peru and Chile, Angola and Namibia, and NW Australia [11]. A limitation of model-based studies, such as [11], is that the vertical resolution of the model grid varies with altitude. For example, the ECMWF L60 vertical grid used in [11] varies at ∼25 m near the surface, ∼300 m at a 1.5 km altitude, ∼500 m at a 4 km altitude, and ∼685 m at a 8 km altitude [12]. Hence, elevated shallow ducts that are few tens of meters thick are not resolvable in the model.

In this paper, we addressed the prevalence and characteristics of observed ducts both at the surface and aloft using a high vertical resolution (∼5 m) upper air sounding data set. These high-resolution soundings provide new details on shallow ducting layers in the atmosphere that are not possible to resolve with lower vertical resolution observations or model outputs. Information on the geography and altitudes of frequent refractivity conditions conducive for ducting is useful for navigation, communication, and weather radar, as well as for defensive and offensive military applications [6,13].

## 2. Materials and Methods

We used upper air soundings with a native vertical resolution of ∼5 m from selected sites in the United States, its territories, and several Pacific islands. Data are from the period of 1 January 2019 to 31 December 2022. In total, atmospheric profiles were analyzed for 49,239 upper air soundings, 23,806 of which contained one or more ducts (Table 1). We analyzed profiles from 7 island sites, 4 coastal sites, 3 sites around the Great Lakes, and 4 inland sites (Figure 1, Table 2). These categories represent varying geographic settings that influence atmospheric properties and ducting behavior. At coastal locations, offshore flow and alongshore flow can yield surface-based ducts, and onshore flow can yield both surface-based and ducts aloft [14]. Previous work has not examined observed duct characteristics at multiple tropical island locations. While the lowest sounding levels are island-influenced, once the sounding is a few km downwind of the island, the conditions are more representative of open ocean.

**Table 1.** Upper air sounding sample sizes and total duct counts for ducts with a >40 m thickness and $M > 1.7$ at 18 locations over 4 years (2019–2022) by location type.

| Location Type | Total Soundings | # of Soundings with ≥1 Duct | Percent of Soundings with ≥1 Duct | Duct Count |
|---|---|---|---|---|
| Island | 19,524 | 11,538 | 59.1% | 32,352 |
| Coastal | 8850 | 6338 | 71.6% | 12,938 |
| Lake | 8871 | 2367 | 26.7% | 3508 |
| Inland | 11,992 | 3565 | 29.7% | 5403 |

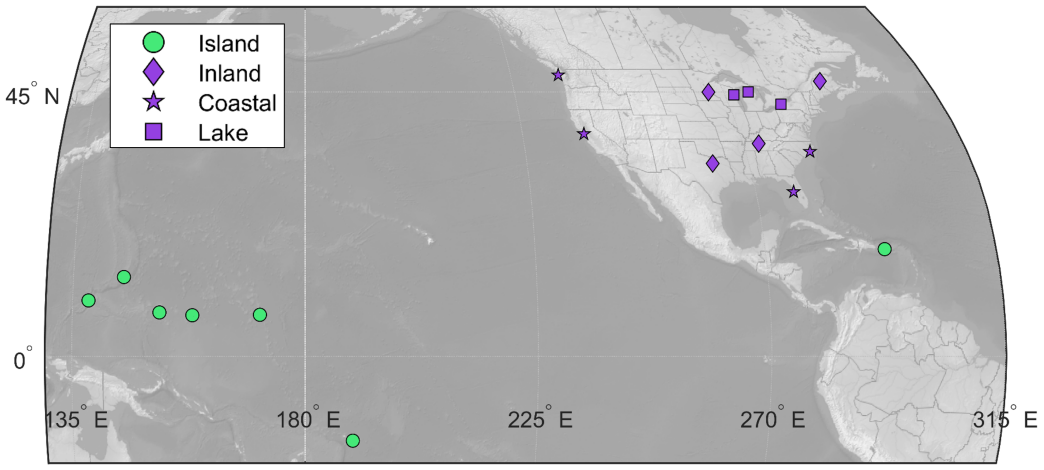


**Figure 1.** Locations of the upper air sounding data used for refractivity profile EM duct analysis. Location type is distinguished by marker type. Color indicates groupings of a location type.

**Table 2.** The upper air sounding locations subset into a corresponding location type: tropical and subtropical island, US coastal, Great Lake, and US inland. The latitude and longitude coordinates and local times at 00 and 12 UTC are listed for each location. For sites that participate in daylight savings, the first local time listed is daylight standard time and the second is daylight savings time.

| Location Name | Latitude (°) | Longitude (°) | Local Time at 00 UTC | Local Time at 12 UTC |
|---|---|---|---|---|
| | | Island | | |
| American Samoa | −14.33 | −170.71 | 1300 | 0100 |
| Chuuk | 7.46 | 151.84 | 1000 | 2200 |
| Guam | 13.48 | 144.80 | 1000 | 2200 |
| Marshall Islands | 7.06 | 171.27 | 1200 | 0000 |
| Micronesia | 6.99 | 158.21 | 1100 | 2300 |
| Puerto Rico | 18.22 | −66.59 | 2000 | 0800 |
| Yap | 9.50 | 138.08 | 1000 | 2200 |
| | | Coastal | | |
| Oakland, CA | 37.80 | −122.27 | 1600/1700 | 0400/0500 |
| Newport, NC | 34.79 | −76.86 | 1900/2000 | 0700/0800 |
| Quilayute, WA | 47.94 | −124.54 | 1600/1700 | 0400/0500 |
| Tampa, FL | 27.95 | −82.46 | 1900/2000 | 0700/0800 |
| | | Lake | | |
| Buffalo, NY | 42.89 | −78.88 | 1900/2000 | 0700/0800 |
| Gaylord, MI | 45.03 | −84.67 | 1900/2000 | 0700/0800 |
| Green Bay, WI | 44.51 | −88.01 | 1800/1900 | 0600/0700 |
| | | Inland | | |
| Caribou, ME | 46.86 | −68.00 | 1900/2000 | 0700/0800 |
| Fort Worth, TX | 32.76 | −97.33 | 1800/1900 | 0600/0700 |
| Minneapolis, MN | 44.98 | −93.27 | 1800/1900 | 0600/0700 |
| Nashville, TN | 36.16 | −86.78 | 1800/1900 | 0600/0700 |

The sounding data were archived by the National Centers for Environmental Information (NCEI) in Binary Universal Form for the Representation of meteorological data (BUFR) format [15,16]. Operational upper air soundings were launched at ∼11 UTC and ∼23 UTC

to achieve mid troposphere altitudes at 0 and 12 UTC each day. The data set we used spans 10 time zones, yielding differences in the local times among the sites (Table 2). We did not have adequate temporal sampling to analyze diurnal cycle variations.

The observed upper air sounding profiles at a ~5 m native resolution were linearly interpolated to 20 m vertical layers in order to standardize the altitude levels. The interpolated data were input into the calculation of modified refractivity ($M$). We used the Python (version 3.10.9) library function numpy.interp (version 1.24.2) to perform 1D linear interpolation based on the geographic heights of the target level and the raw data. The combined uncertainty, including calibration and accuracy, of the sondes' Vaisala temperature sensor was 0.3 °C, and the combined uncertainty of the relative humidity sensor was 4% [17].

Modified refractivity is a function of temperature, water vapor, pressure, and the curvature of the Earth. The advantage of modified refractivity over refractivity is that all negative $M$ vertical gradients are associated with trapping layers, which simplifies duct identification [4,7]. Modified refractivity ($M$) is determined using the following equation:

$$M = \frac{77.6}{T}\left(P + \frac{4810e}{T}\right) + \frac{z}{10^{-6}R_e}, \quad (1)$$

where $P$ is pressure (mb), $T$ is temperature (K), $e$ is vapor pressure (mb), $z$ is height (m), and $R_e$ is the radius of the Earth (m) [2,18]. Modified refractivity values were calculated for each height level in each sounding.

Figure 2 illustrates the key components and characteristics of a wave duct as a function of modified refractivity and altitude. A trapping layer is characterized by a decrease in modified refractivity with increasing height [14]. The thickness of an elevated duct is the distance between the local minimum in $M$ above the trapping layer to the same value of $M$ below the trapping layer. Surface-based ducts only have the trapping layer portion, in which case, the duct thickness is defined as the trapping layer thickness. Observed examples of modified refractivity profiles are annotated with the trapping layer top and bottom and duct base in Figure 3. The example from Guam at 1106 UTC on 31 March 2022 contained seven ducts aloft (Figure 3a). A surface duct along with three ducts aloft is shown in the example from Wallops Island, VA, at 2300 UTC on 11 July 2022 (Figure 3b).

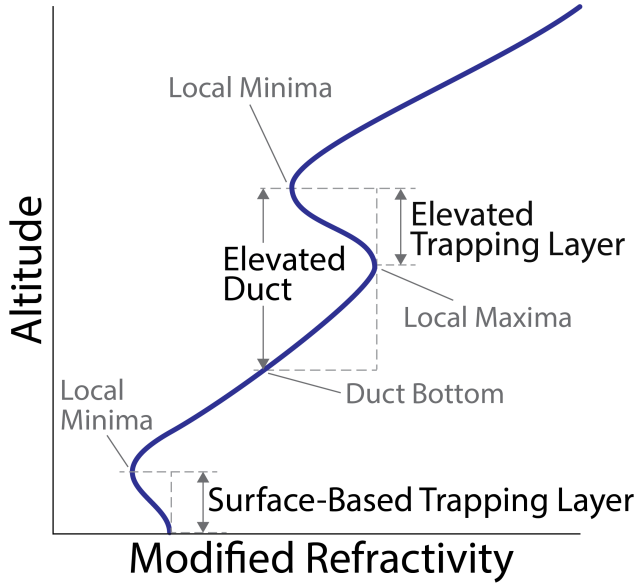


**Figure 2.** Idealized schematic of the electromagnetic wave duct components as a function of modified refractivity and height (adapted from [13,14]).

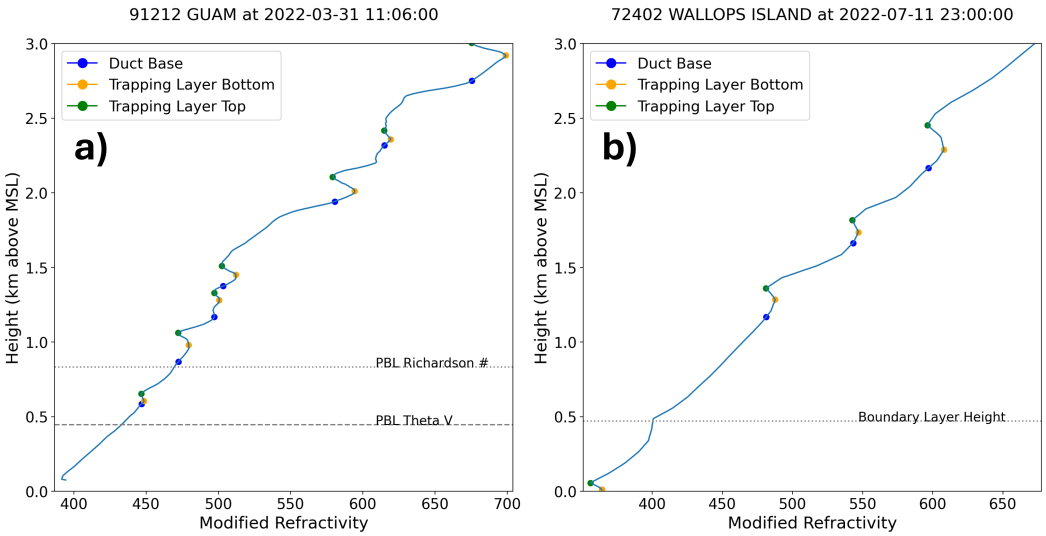


**Figure 3.** Modified refractivity profiles from (**a**) Guam on 1106 UTC 31 March 2022 with multiple ducts aloft; and (**b**) Wallops, VA on 2300 UTC 11 July 2022 with multiple ducts aloft and a surface duct. The planetary boundary layer height based on the Richardson number and on virtual potential temperature (Theta V) [19] differed, as shown in (**a**), and are shown separately. As shown in (**b**), both estimates of the boundary layer height were found to be at the same altitude.

Using the information on the trapping layer top and bottom and duct base, we calculated the duct strength as the difference between the local maxima in $M$ at the trapping layer bottom and the local minima in $M$ at the trapping layer top. Two thresholds were applied to filter out very weak or very thin modified refractivity inversions. A duct was included in the analysis only if it met both the criteria of a duct strength of $M > 1.7$ and a duct thickness of >40 m. The thickness threshold of 40 m represents two adjacent 20 m layers. The gradient magnitudes were spatial scale-dependent. The specific thresholds were based on our judgment of adequacy for the purpose [20] of the input data set and examination of the distributions of the M values and thicknesses. By focusing on these features, this study aimed to provide improved understanding of the electromagnetic wave duct frequency of occurrence and variations across different environments. A user of our duct inventory can choose to threshold at higher values of thickness and M dependent on their application.

## 3. Results

Most atmospheric profiles at the coastal (72%) and island (59%) locations had one or more ducts (Table 1). In comparison, the lake and inland profiles had one or more ducts in less than 30% of the time. Multiple ducts per profile are more likely in island locations (Figure 4). Statistics for duct characteristics by location type are presented in Table 3. The median duct strengths (∼4.1 to 4.7 M) and thicknesses (∼100 m) were similar among the location types. The distributions of the duct base altitudes showed notable differences among the location types, with the median value for islands (1781 m) about 1 km higher in altitude than for the coastal (874 m) regions. As a consequence, the median duct top altitudes were also about 1 km higher for the island as compared to the coastal sites. The Great Lake and inland locations had median duct base altitudes of 1128 m and 1320 m, respectively, at intermediate values between the island and coastal values. The increased height of the ducts between the US coastal versus subtropical and tropical islands was found to be consistent with the increasing height of the inversion-topped marine boundary layer documented along the ship transects that traversed from marine stratocumulus to trade cumulus conditions between Southern California and Hawaii [21].

**Table 3.** The median and the 10th, 25th, 75th, and 90th percentiles for the duct characteristics of strength, thickness, duct base height, and duct top height for each location type.

| | 10th | 25th | Median | 75th | 90th |
|---|---|---|---|---|---|
| Strength (*M*) | | | | | |
| Island | 2.04 | 2.66 | 4.13 | 7.23 | 12.40 |
| Coastal | 2.10 | 2.83 | 4.69 | 8.69 | 15.11 |
| Lake | 2.03 | 2.69 | 4.23 | 7.46 | 12.42 |
| Inland | 2.05 | 2.70 | 4.35 | 8.19 | 14.46 |
| Thickness (m) | | | | | |
| Island | 52 | 66 | 94 | 156 | 257 |
| Coastal | 55 | 73 | 114 | 191 | 298 |
| Lake | 54 | 72 | 104 | 164 | 238 |
| Inland | 58 | 76 | 113 | 179 | 276 |
| Duct Base Height (m) | | | | | |
| Island | 503 | 963 | 1781 | 2628 | 3589 |
| Coastal | 55 | 324 | 874 | 1730 | 2720 |
| Lake | 41 | 460 | 1128 | 1826 | 2599 |
| Inland | 83 | 649 | 1320 | 2060 | 2867 |
| Duct Top Height (m) | | | | | |
| Island | 627 | 1098 | 1935 | 2750 | 3689 |
| Coastal | 219 | 512 | 1018 | 1887 | 2720 |
| Lake | 177 | 579 | 1272 | 1969 | 2708 |
| Inland | 228 | 810 | 1490 | 2198 | 2975 |

The inter-relationships among the heights, thicknesses, and strength of the ducts observed between the locations are illustrated in Figures 5–7. Most ducts are not surface-based (Figure 5) as 75% have tops within the first 3 km of the surface and 75% have thicknesses of 200 m or less (Figure 6, Table 3). As duct thickness increases to >200 m, the range of duct strengths tends to broaden to include higher value outliers. While thin ducts tend to be weak (M < 10), the high prevalence of weak, thick ducts yields linear correlations that explain less than half the variance between duct strength and and thickness (Figure 6). Since the correlations were low, we do not recommend using these linear fits to parameterize the relationship between duct strength and thickness for different location types. There was no meaningful linear correlation found between the duct strength and height (Figure 7).

The surface-based ducts represent a combination of the evaporative downdrafts reaching the surface, nocturnal radiation cooling, and sea breezes in the coastal, lake, and island locations. Nocturnal radiation inversions are more likely to form on calm, clear nights at inland locations than near bodies of water. The onshore movement of a low layer of cooler ocean air in the afternoon associated with the sea breeze (or a lake breeze) would be conducive to ducting.

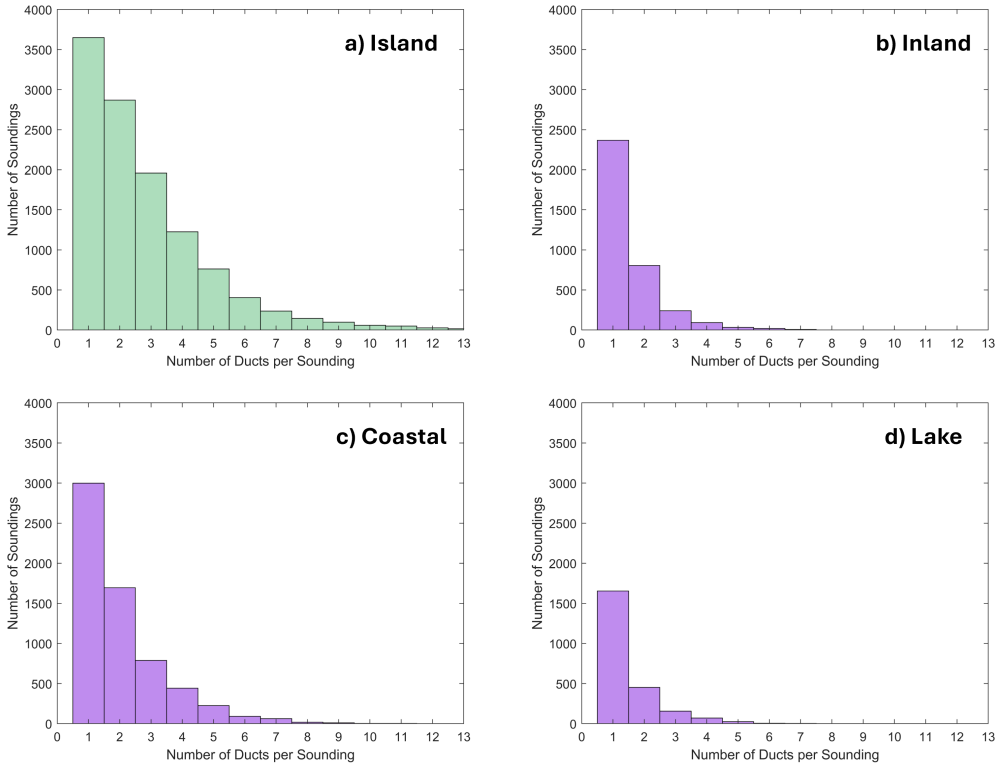


**Figure 4.** Distributions of the number of ducts in a given sounding for the (**a**) tropical and subtropical island, (**b**) US inland, (**c**) US coastal, and (**d**) Great Lake locations. For the island locations, 39 soundings had more than 13 ducts.

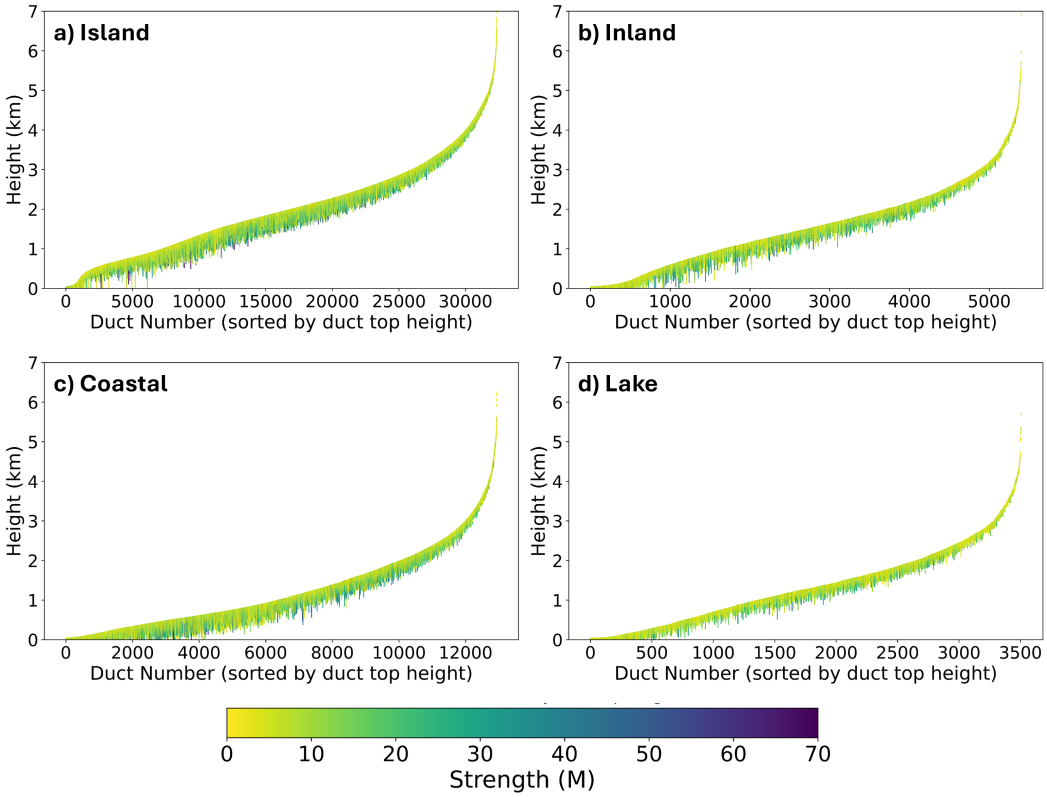


**Figure 5.** The EM duct thickness (vertical length of line) and strength (color-coded) sorted by duct top height for the (**a**) tropical and subtropical island, (**b**) US inland, (**c**) US coastal, and (**d**) Great Lake locations. For the island locations, 13 ducts had duct top heights exceeding 7 km.

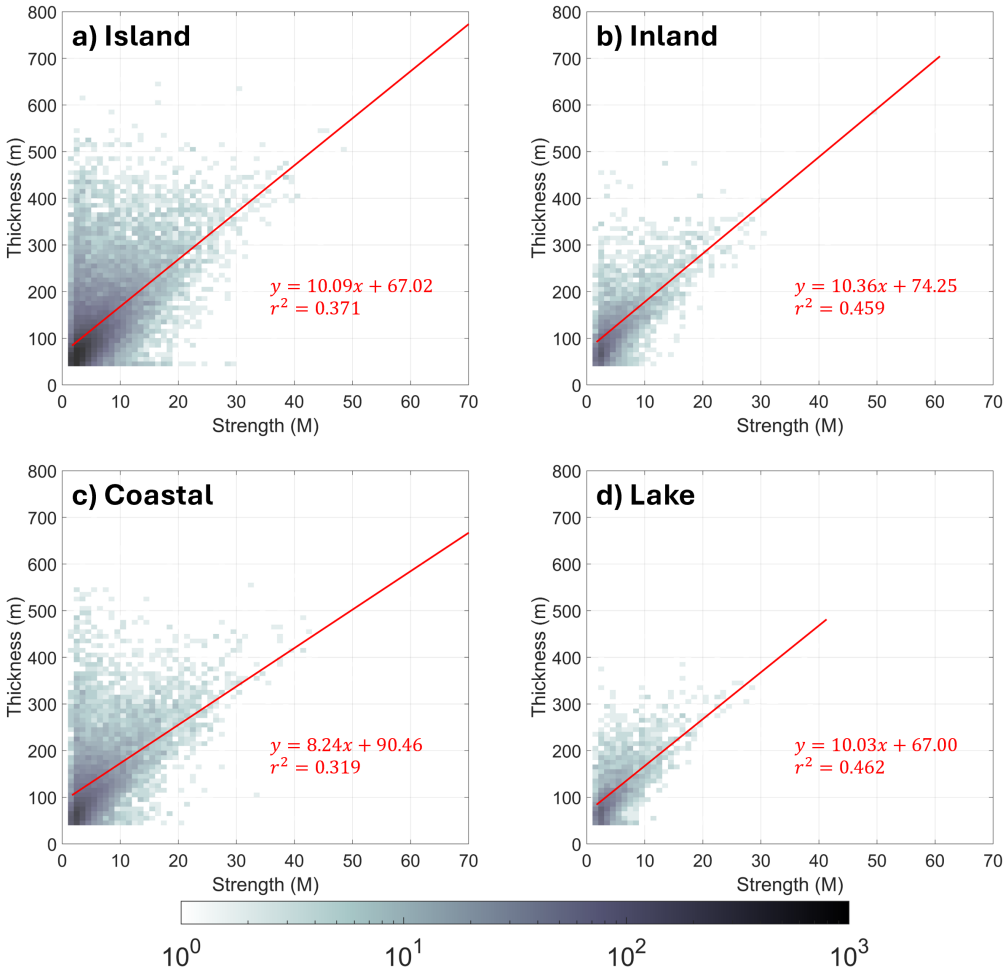


**Figure 6.** Scatter density plots of the duct thickness (m) vs. strength (M) for the (**a**) tropical and subtropical island, (**b**) US inland, (**c**) US coastal, and (**d**) Great Lake locations. The linear regression line (red), corresponding equation, and the coefficient of determination ($r^2$) are displayed on each subplot. Shading indicates the number of samples.

The range of surface-based duct strengths was found to be similar to that for the elevated ducts (Figure 7). There were a few outliers with $M > 30$ in each location category.

The frequency of occurrence of soundings with ducts in different atmospheric layers (surface, between surface, 2 km, and $\geq$2 km altitude) is tabulated in Table 4. If a particular sounding had a surface-based duct and one duct above 2 km it would be counted in each of those categories. The island locations stood out with many more soundings containing ducts above a 2 km altitude (61%) compared to the other locations (<31%), which is discussed further in Section 4.

Based on our data analysis, the duct characteristics from US coastal measurements were usually not representative of the tropical open ocean conditions. Compared to coastal ducts, the distribution of subtropical and tropical island duct heights were shifted to higher altitudes (Figures 5 and 7, Table 3). Island locations were found to be more likely to have stronger ducts ($M > 25$) at altitudes above 1 km than coastal locations (Figure 7). The frequency of surface-based ducts was lower on islands (2%) compared to coastal locations (10%) (Table 4).

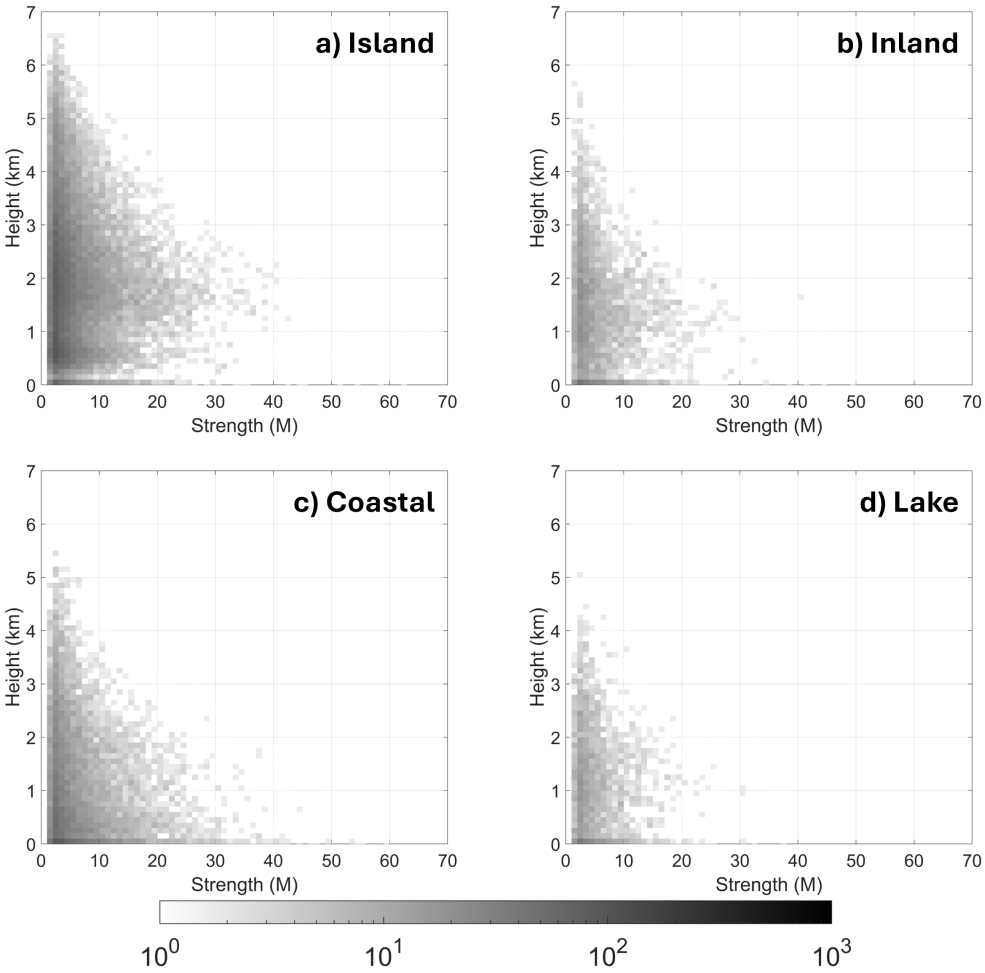


**Figure 7.** Scatter density plots of the duct base height (km) vs. strength (*M*) for the (**a**) tropical and subtropical island, (**b**) US inland, (**c**) US coastal, and (**d**) Great Lake locations. Shading indicates the number of samples.

**Table 4.** The counts and percentages of the duct occurrences in different layers of the atmosphere based on location type. In most circumstances, altitudes of >2 km would have been above the boundary layer height [19]. The percentages are relative to the total number of soundings with one or more ducts for a location type (Table 1).

| Criteria | Island | Coastal | Lake | Inland |
|---|---|---|---|---|
| Includes a surface-based duct | 281 (2.4%) | 631 (10.0%) | 283 (12.0%) | 393 (11.0%) |
| Includes $\geq$ 1 duct with base > surface and <2 km | 8724 (75.6%) | 5233 (82.6%) | 1829 (77.3%) | 2600 (72.9%) |
| Includes $\geq$ 3 ducts with base > surface and <2 km | 1475 (12.8%) | 1125 (17.8%) | 140 (5.9%) | 189 (5.3%) |
| Includes $\geq$ 1 duct $\geq$ 2 km altitude | 7051 (61.1%) | 1855 (29.3%) | 602 (25.4%) | 1120 (31.4%) |
| Includes $\geq$ 3 ducts $\geq$ 2 km altitude | 1637 (14.2%) | 132 (2.1%) | 25 (1.1%) | 51 (1.4%) |

## 4. Discussion

For the island locations, surface-based ducts and ducts associated with inversions near boundary layer tops were expected. However, the high prevalence of ducts with bases above the boundary layer height (a duct base with a >2 km altitude) was not expected

(Figures 5 and 7 and Table 4). Ducts are stable layers; as such, a key question is what are the likely mechanisms producing stable layers of ≥a 2 km altitude in tropical and subtropical oceanic settings? Subtropical marine regions have persistent large-scale subsidence associated with the downward branch of the Hadley circulation. The subsidence manifests as temperature inversions and humidity gradients yielding trade wind cumulus clouds over warmer oceans and stratocumulus clouds over cooler oceans [22,23]. However, large-scale subsidence would not readily explain the multiple ducts aloft at different altitudes in the same sounding, as illustrated in Figure 3a. In the 24 hours prior to the sounding, Guam hourly METARS reported up to three distinct cloud layers, with bases ranging between 600–2700 m. At any one time in a marine cumulus cloud field, clouds are forming and dissipating. Some small cumulus clouds produce precipitation that reaches the surface but most do not. Some cumulus yield virga that will cool and moisten the air just below cloud base. Dry air entrainment dissipates clouds and moistens and cools the immediate vicinity (see, e.g., [24]). Layer moistening by cumulus cloud dissipation is implicated in the multi-week transition between the suppressed (dry) and active (wet) phases of the Madden–Julian oscillation (see, e.g., [25]). Over hourly to daily time scales, layer moistening by cloud detrainment and virga may have implications for the creation of ∼100 m thick stable layers and, potentially, ducts if the moisture gradient persists. Determining the physical mechanisms that yield multiple ducts aloft in these settings requires in-depth study with more data.

## 5. Conclusions

Our analysis of more than 49,000 modified refractivity profiles derived from 20 m vertical resolution upper air sounding data complements previous studies on EM duct characteristics based on coarser vertical resolution modeling and observations. By examining a large data set from geographically diverse sites, we are able to discern the similarities and differences among ducts in different environments. The key findings from observed profiles of modified refractivity, including ducts that were at least 40 m in thickness and with strengths of $M \geq 1.7$, are as follows:

- In all of the location types, elevated ducts were found to be more common than surface-based ducts.
- The median values of the duct strengths ($M$ between 4.1 and 4.7) and thicknesses (∼100 m) were similar across location types.
- Duct strength tended to increase with increasing duct thickness, but this relationship explained less than half of the variance.
- The duct strength and duct base height were not correlated.
- Profiles with one or more ducts were common at the tropical and subtropical island (∼60%) and US coastal locations (∼70%), and they occurred less than 30% of the time at the Great Lakes and US inland sites.
- Notable differences between the ducts at tropical and subtropical islands versus the US coastal locations included islands that had higher median duct base altitudes, a higher frequency of stronger ducts at altitudes of > 1 km, and a lower frequency of surface-based ducts.
- The tropical and subtropical island locations often exhibited one or more elevated ducts above a 2 km altitude in a single profile—a phenomena requiring further investigation.

Whereas previous work has focused on surface-based EM ducts and those associated with inversion-topped boundary layers, our 20 m vertical scale data set permitted investigation of these kinds of ducts, as well as those above the boundary layer. Our analysis revealed a wide variety of strengths and heights of naturally occurring shallow elevated EM ducts (Figures 5–7). The wide joint frequencies of the characteristics presented

challenges in terms of simplifying duct characteristics into idealized representative cases. The previously unrecognized prevalence of elevated ducts above a 2 km altitude is relevant for the performance of active and passive remote sensing from aircraft and surface-based sensors. In the future, the duct inventory we have posted on a public archive can be used as an input to radar propagation models to determine the impacts of the observed ducts aloft and at the surface on beam paths for different EM applications.

**Author Contributions:** Conceptualization, S.E.Y. and M.A.M.; methodology, K.D.B. and M.M.S.; software, K.D.B. and M.M.S.; validation, K.D.B. and S.E.Y.; resources, M.A.M.; data curation, K.D.B. and S.E.Y.; writing—original draft preparation, S.E.Y. and M.M.S.; writing—review and editing, S.E.Y., M.A.M., K.D.B., and M.M.S.; visualization, S.E.Y., M.M.S., and M.A.M.; supervision, S.E.Y.; project administration, S.E.Y.; funding acquisition, S.E.Y. and M.A.M. All authors have read and agreed to the published version of the manuscript.

**Funding:** Research supported by the Office of Naval Research (grants N00014-21-1-2116 and N00014-24-1-2216).

**Institutional Review Board Statement:** Not applicable.

**Informed Consent Statement:** Not applicable.

**Data Availability Statement:** Data available in a publicly accessible archive. Upper-air sounding data used in this analysis are available from NCEI at https://www.ncei.noaa.gov/data/nws-global-upper-air-bufr/ (accessed on 1 March 2023). Data files listing all of the identified ducts and their key characteristics are available at https:doi.org/10.17605/OSF.IO/4THR5.

**Acknowledgments:** Special thanks to Matt Wilbanks, Tim Whitcomb, Teddy Holt, and James Doyle for their feedback and comments. We would also like to thank the anonymous reviewers of the manuscript whose comments helped us to clarify and refine the material in this paper. The views expressed in this article are those of the authors and do not necessarily reflect the official policy or position of the United States Air Force Academy, the Air Force, the Department of Defense, or the U.S. Government. Approved for public release: distribution unlimited. USAFA-DF-2025-28.

**Conflicts of Interest:** The authors declare no conflicts of interest.

## References

1. Kerr, D.E. *Propagation of Short Radio Waves*, 1st ed.; Number 13 in Radiation Laboratory; McGraw-Hill Book Company Inc.: New York, NY, USA, 1951.
2. Bean, B.R.; Dutton, E.J. *Radio Meteorology*; Dover Publications: Garden City, NY, USA, 1966.
3. Rosenthal, J. *Refractive Effects Guidebook*; COMTHIRDFLT TACMEMO 280-1-76; Naval Ocean Systems Center: San Francisco, CA, USA, 1979. Available online: https://apps.dtic.mil/sti/tr/pdf/ADA034073.pdf (accessed on 16 December 2024).
4. Kukushkin, A. *Radio Wave Propagation in the Marine Boundary Layer*; Wiley: New York, NY, USA, 2004.
5. Cairns-McFeeters, E.L. Effects of Surface-Based Ducts on Electromagnetic Systems. Master's Thesis, Naval Post Graduate School, Monterey, CA, USA, 1992.
6. Turton, J.D.; Bennetts, D.A.; Farmer, S.F.G. An introduction to radio ducting. *Meteorol. Mag.* **1988**, *117*, 245–254.
7. Saeger, J.T.; Grimes, N.G.; Rickard, H.E.; Hackett, E.E. Evaluation of simplified evaporation duct refractivity models for inversion problems. *Radio Sci.* **2015**, *50*, 1110–1130. [CrossRef]
8. Thompson, W.T.; Haack, T. An Investigation of Sea Surface Temperature Influence on Microwave Refractivity: The Wallops-2000 Experiment. *J. Appl. Meteorol. Climatol.* **2011**, *50*, 2319–2337. [CrossRef]
9. Alappattu, D.P.; Wang, Q.; Yamaguchi, R.T.; Haack, T.; Ulate, M.; Fernando, H.J.; Frederickson, P. Electromagnetic Ducting in the Near-Shore Marine Environment: Results From the CASPER-East Field Experiment. *J. Geophys. Res. Atmos.* **2022**, *127*, e2022JD037423. [CrossRef]
10. Doyle, J.D.; Patel, R.N.; Reynolds, C.; Cobb, A. Impact of Atmospheric Rivers on Electromagnetic Ducting as Diagnosed from Dropsondes. *J. Appl. Meteorol. Climatol.* 2025, *conditionally accepted*.
11. von Engeln, A.; Teixeira, J. A ducting climatology derived from the European Centre for Medium-Range Weather Forecasts global analysis fields. *J. Geophys. Res. Atmos.* **2004**, *109*, D18104. [CrossRef]

12. ECMWF. *European Center for Medium-Range Weather Forecasts (ECMWF) Model Level Definitions*; ECMWF: Reading, UK, 2024. Available online: https://confluence.ecmwf.int/display/UDOC/Model+level+definitions (accessed on 16 December 2024).
13. Cherrett, R.C. Capturing Characteristics of Atmospheric Refractivity Using Observations and Modeling Approaches. Ph.D. Thesis, Naval Postgraduate School, Monterey, CA, USA, 2015.
14. Haack, T.; Wang, C.; Garrett, S.; Glazer, A.; Mailhot, J.; Marshall, R. Mesoscale Modeling of Boundary Layer Refractivity and Atmospheric Ducting. *J. Appl. Meteorol. Climatol.* **2010**, *49*, 2437–2457. [CrossRef]
15. NCEI. *Global BUFR Data Stream: Upper Air Reports from the National Weather Service Telecommunications Gateway (NWS TG)*; NCEI: Asheville, NC, USA, 2021. Available online: https://www.ncei.noaa.gov/access/metadata/landing-page/bin/iso?id=gov.noaa.ncdc:C01500;view=iso#idm140422537286768 (accessed on 16 December 2024).
16. World Meteorological Organization. *WIS Manuals*; World Meteorological Organization: Geneva, Switzerland, 2022. Available online: https://community.wmo.int/activity-areas/wis/wis-manuals (accessed on 16 December 2024).
17. Vaisala. *Radiosonde RS41-SGE with BioCover*; Vaisala: Vantaa, Finland, 2023. Available online: https://docs.vaisala.com/v/u/B212709EN-A/en-US (accessed on 16 December 2024).
18. Brooks, I.M.; Goroch, A.K.; Rogers, D.P. Observations of Strong Surface Radar Ducts over the Persian Gulf. *J. Appl. Meteorol.* **1999**, *38*, 1293–1310. [CrossRef]
19. Stull, R.B. *An Introduction to Boundary Layer Meteorology*; Springer: Dordrecht, The Netherlands, 1988.
20. Parker, W.S. Model Evaluation: An Adequacy-for-Purpose View. *Philos. Sci.* **2020**, *87*, 457–477. [CrossRef]
21. Alappattu, D.P.; Wang, Q.; Kalogiros, J. Anomalous propagation conditions over eastern Pacific Ocean derived from MAGIC data. *Radio Sci.* **2016**, *51*, 1142–1156. [CrossRef]
22. Stevens, B. Atmospheric Moist Convection. *Annu. Rev. Earth Planet. Sci.* **2005**, *33*, 605–643. [CrossRef]
23. de Szoeke, S.P.; Verlinden, K.L.; Yuter, S.E.; Mechem, D.B. The Time Scales of Variability of Marine Low Clouds. *J. Clim.* **2016**, *29*, 6463–6481. [CrossRef]
24. Gerber, H.E.; Frick, G.M.; Jensen, J.B.; Hudson, J.G. Entrainment, Mixing, and Microphysics in Trade-Wind Cumulus. *J. Meteorol. Soc. Jpn. Ser. II* **2008**, *86A*, 87–106. [CrossRef]
25. Riley, E.M.; Mapes, B.E.; Tulich, S.N. Clouds Associated with the Madden–Julian Oscillation: A New Perspective from CloudSat. *J. Atmos. Sci.* **2011**, *68*, 3032–3051. [CrossRef]